Stability of irradiation-induced point defects on walls of carbon nanotubes

A. V. Krasheninnikov[a] and K. Nordlund
Accelerator Laboratory, University of Helsinki, P.O. Box 43, FIN-00014, Finland

(Received 2 October 2001; accepted 30 January 2002)

Using empirical-potential and tight-binding models, we study the structure and stability of atomic-scale irradiation-induced defects on walls of carbon nanotubes. Since atomic vacancies are the most prolific but metastable defects which appear under low-dose, low-temperature ion irradiation, we model the temporal evolution of single vacancies and vacancy-related defects (which isolated vacancies can turn into) and calculate their lifetimes at various temperatures. We further simulate scanning-tunneling microscopy (STM) images of irradiated nanotubes with the defects, employing for this the tight-binding Green's function technique. Our simulations demonstrate that the defects live long enough at low temperatures to be detected by STM and that different defects manifest themselves in STM images in different ways, all of which makes it possible to detect and distinguish the defects experimentally. © *2002 American Vacuum Society.*
[DOI: 10.1116/1.1463728]

I. INTRODUCTION

Of late, numerous experimental and theoretical studies on carbon nanotubes have demonstrated possibilities for developing carbon-based electronics.[1–5] However, implementation of even the simplest electronic devices demands a thorough understanding of the structural and electronic properties, not only of perfect nanotubes, but also of nanotubes with various defects which can appear during nanotube growth or can be created by external actions. Moreover, recent experiments[5] indicate that the defects in nanotubes can be used to fabricate an intratube quantum dot device. However, methodological development requires knowing what the defects involved are, and how they can be produced in a controllable way. Besides this, the studies on imperfect nanotubes are of particular interest due to a unique opportunity to investigate the influence of disorder on properties of genuine one-dimensional systems of nearly macroscopic size.

Thus, many theoretical and experimental works on the electronic and structural properties of nanotubes with defects[6–17] and on the formation of defects under electron[18–21] or ion irradiation[22–24] have recently appeared. Various point defects in nanotubes have been considered, such as pentagon/heptagon Stone-Wales defects associated with a rotation of a bond in the nanotube atom network,[6–10] adatoms on the walls of nanotubes,[11] impurities,[12] and defects initiated through the adsorption of a carbon dimer on a nanotube wall.[10,17] A large number of theoretical works deal with atomic vacancies.[12–16,19,22,23]

At the same time, it is not yet quite clear whether the atomic vacancies exist in carbon nanotubes or not. Although, as recent studies demonstrate,[19,22,23] single vacancies and vacancy clusters may be created by removing carbon atoms by knock-on events under electron or ion irradiation, such defects may be metastable or even quite unstable transforming quickly to other defects.

Indeed, recent experiments indicate that high-dose electron[18,19] irradiation of single-walled nanotubes (SWNTs) gives rise to surface reconstructions and drastic dimensional changes, as a corollary of which the apparent diameters of SWNT's substantially shrink. To explain these phenomena, it has been suggested[19] that isolated vacancies (which appear under irradiation) are unstable and the apparent reduction of the SWNT diameter is due to a mending of the vacancies through dangling bond saturation and by forming vacancy-related defects such as nonhexagonal rings or pentagon-one-dangling-bond defects.

Tight-binding molecular dynamics simulations[19] conducted at a temperature of 700 K confirm the vacancy-mending mechanism for high irradiation beam dose (when a large number of atoms are removed very rapidly) and at high temperatures. However, because of an extremely high rate of atom removal (of 5 atoms/ps), that study is not relevant to ordinary ion irradiation dose rates. Moreover, it is not quite clear whether single vacancies also transform easily at low temperatures and how the lifetime of vacancies depends on the temperature. Besides this, recent experimental work[24] on the irradiation of nanotubes with Ar ions indicate that dangling bonds are present in irradiated nanotubes. Since dangling bonds are usually related to isolated vacancies, such vacancies, even if metastable, may be long-lived defects (and may survive for macroscopic times), especially under low-temperature, low-dose irradiation. It should be noted, however, that the dangling bonds may also be associated with the other vacancy-related defects which have been considered in Ref. 19. Thus, the stability of vacancies and vacancy-related defects as well as their influence on the electronic properties of SWNTs call for further studies.

Recently we demonstrated[23] that vacancies are the predominant defects which appear under low-energy irradiation of individual single-wall nanotubes with Ar ions. We also showed that ideal single vacancies at low temperatures are metastable but macroscopically long-lived defects. Since a scanning tunneling microscope (STM) is a good tool to iden-

[a]Author to whom correspondence should be addressed; electronic mail: akrashen@beam.helsinki.fi

tify atom-scale defects at surfaces directly, we also simulated STM images of irradiated nanotubes with ideal vacancies within the framework of a tight-binding approach. Out results show that the vacancies may be detected by STM and that, at low bias voltages, they appear as bright spots in the STM images due to the growth in the local electron density of states on atoms surrounding the defects. However, we did not study the stability of the vacancy-related defects, or simulat their STM images or current-to-voltage characteristics.

In this article, making use of molecular dynamics with empirical potentials,[26] we (i) study the stability and temporal evolution of vacancy-related defects in SWNTs, (ii) present the details of our calculations on the ideal vacancy stability (which were omitted in Ref. 23), and (iii) simulate STM images of SWNTs and STM current-to-voltage characteristics in the vicinity of the vacancy-related defects. We (iv) further discuss possible STM experiments on real-time monitoring of the time evolution of irradiation-induced defects on the walls of carbon nanotubes, since such experiments may not only contribute to understanding the mechanisms of defect formation, but may also serve as a test for the validity of tight-binding and empirical potential molecular dynamics models.

II. CALCULATIONS OF THE VACANCY-RELATED DEFECT LIFETIMES WITHIN THE FRAMEWORK OF EMPIRICAL POTENTIAL MODELS

In Ref. 23 we have studied formation probabilities of atomic-scale defects produced by low-dose irradiation of nanotubes with Ar ions. We have considered (10,10) armchair SWNTs, which are reported to be the predominant constituents of ropes synthesized by the electric arc technique using a catalyst.[28] Using molecular dynamics,[25] we have simulated impact events over a wide energy range of incident ions. We have shown that the most common defects produced under ion irradiation are vacancies, which at low temperatures are metastable but long-lived defects.

At high temperatures the vacancies (ideal vacancies which have three dangling bonds) can transfer to two other defects. Those are single pentagon-one dangling bond atomic configurations and fourfold coordinated atoms in the center of two pentagons and two hexagons, cf. Fig. 1. For brevity, we label the former defect ''5-1db'' and the latter ''5-6'' defect. Formations of such defects under high-dose electron irradiation have also been reported.[19]

The tight-binding and empirical potential simulations indicate that the 5-1db defect has the lowest energy.[19,23] Thus, although all three defects may appear as a result of ion impact, the long quenching of the nanotubes should eventually lead to the transformations of single vacancies and 5-6 defects to 5-1db defects. However, since single vacancies and 5-6 defects are metastable (i.e., there is an energy barrier separating these two configurations from the configuration with the minimum energy), such defects may survive at low temperatures for finite times which may be long enough for detecting the defects experimentally.

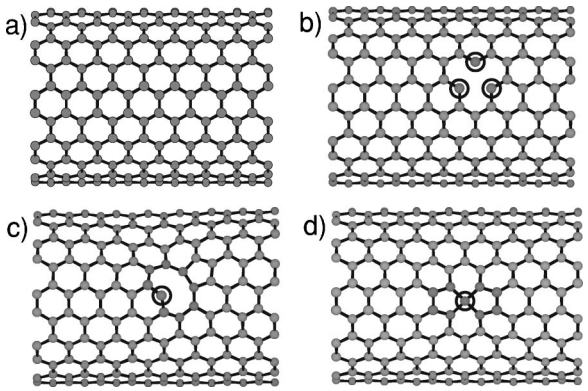

FIG. 1. Ball-and-stick representation of the carbon network of a pristine (10,10) single-walled nanotube (a). Carbon network of the nanotube with an irradiation-induced vacancy (b) as well as vacancy-related defects in ''5-1db'' (c) and ''5–6'' (d) configurations. Only the front walls of the nanotubes are sketched. Atoms with unusual number of bonds are circled.

Our goal here is to estimate the lifetimes of these metastable defects. To examine the stability of the defects, we simulated the time evolution of a 100-Å-long nanotube with the defects over timescales up to more than 10 ns at temperatures of 1000–4000 K employing molecular dynamics.[25] The Brenner potential,[26] without bond conjugation terms, was used for modeling the carbon atom interaction. This potential reproduces well the melting point[27] and elastic constants[26] of graphite and diamond. A good correlation between the results of *ab initio* and classical simulations of nanotubes has also been reported.[11,29]

We found that at high temperatures a single vacancy does transform into 5-6 and 5-1db defects. At least at temperatures below 2500 K, the clearly dominant process was a transformation into the 5-1db defect, as expected from the defect energetics. The vacancy lifetimes at different temperatures are shown in Fig. 2. For every temperature considered, we carried out at least 40 independent runs and averaged the results. With simulations between temperatures of 1500 and 2200 K, we determined that the average vacancy lifetime can be well described with activated behavior with a single activation energy, i.e., by the formula $\tau_{\mathrm{vac}} = a \exp(b/k_B T)$, where

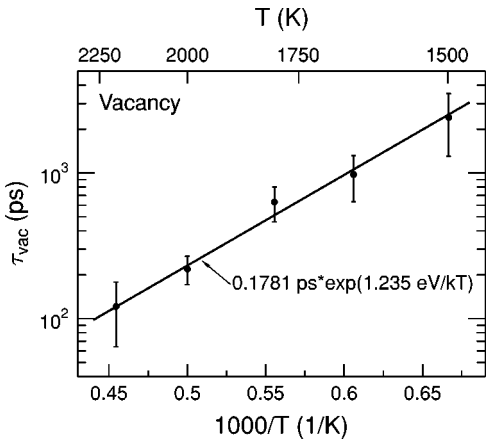

FIG. 2. Lifetimes of single vacancies at different temperatures.

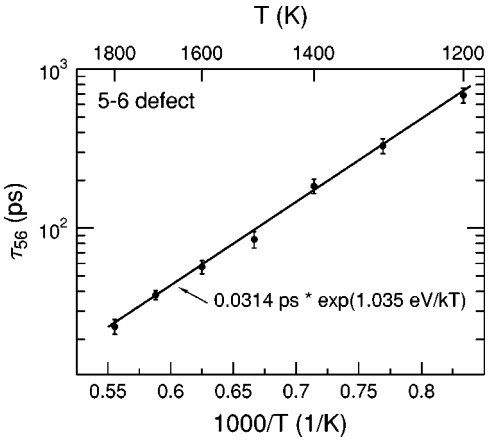

FIG. 3. Lifetimes of 5-6 defects at different temperatures.

τ_{vac} is the time before the vacancy transforms into the 5-1db defect, k_B is Boltzmann's constant, T is the temperature, and a and b are the fitting constants. Our best fit gave $a=0.18\pm0.02$ ps and $b=1.2\pm0.1$ eV.

Thus, empirical potential dynamics simulations indicate that at low temperatures single vacancies are stable on long time scales. If the activation energy for vacancy transformation is $\gtrsim 1$ eV, as our simulations indicate, the vacancies can be expected to be stable at room temperature for time scales of at least the order of 10 h (if we use the formula with the parameters derived above, then we get $\tau=7.2\times10^3$ h). Thus, they might be experimentally found.

We also carried out similar simulations for 5-6 defects in a temperature range of 1200–1800 K. The lifetime τ_{56} of this defect as a function of the temperature is given in Fig. 3. Again, the average lifetime of the defect can be well described with activated behavior with a single activation energy. Our fit gave $a=0.03\pm0.01$ ps and $b=1.04\pm0.01$ eV. The lifetime of 5-6 defects is about 5 h at room temperatures, which is three orders of magnitude shorter than that for vacancies. The difference in the lifetimes is not surprising since the 5-6 defects have higher energies than isolated vacancies, although the energy difference heavily depends on the particular theoretical model used.[23] Thus, 5-6 defects may also potentially survive long enough to be detected experimentally.

Our molecular dynamics simulations carried out within the framework of a tight-binding approximation,[30] gave similar behavior of the defects at high temperatures. However, it proved too computationally expensive to achieve the statistics sufficient for quantitatively describing the activated behavior below 1800 K.

III. TIGHT-BINDING SIMULATIONS OF STM IMAGES OF NANOTUBES WITH IRRADIATION-INDUCED DEFECTS

Having calculated the geometry of the vacancy and vacancy-related defects within the framework of the classical and tight-binding models by minimizing the total energy of the carbon network after defect creation, we computed the STM images of the irradiated SWNTs near these defects within the framework of the tight-binding approximation.

Our technique is based on the formalism developed in Ref. 31. We have successfully used this method for calculations of STM images of graphite surfaces with point defects[32] and carbon nanotubes.[23,33,34] Although our technique has been described at length in those publications, we briefly outline the basics of the method here in order to facilitate understanding the results obtained.

We considered the limit of small bias voltages $V_{\mathrm{bias}}\leqslant 0.5$ V applied to the tip-nanotube interface, and large STM tip sample separations (larger than 4 Å). Since at such separations the tip-surface interaction is weak, a perturbative approach[35] along with the tight-binding Green's function technique[36] may be employed and, to the first order in the tip-nanotube interaction, the tunneling current I as a function of the tip coordinates (x,y,z) may be written[31] at zero temperature as

$$I(x,y,z)=\frac{2\pi e}{\hbar}\int_{E_F}^{E_F+eV_{\mathrm{bias}}} \times\sum_i |V_i(x,y,z)|^2\rho_{\mathrm{tip}}(E)\rho_{\mathrm{tube}}(i,E)\,dE, \qquad (1)$$

where the sum runs over all sites involved in the tip-nanotube hopping. $V_i(x,y,z)$ is the tunneling matrix element coupling the tip apex atom to the atom i of the nanotube, $\rho_{\mathrm{tip}}(E)$ and $\rho_{\mathrm{tube}}(i,E)$ are the local density of states (LDOS) of the noninteracting tip and the nanotube, respectively. The STM tip was modeled as the final atom of a semi-infinite, one-dimensional chain, which made it possible to calculate $\rho_{\mathrm{tip}}(E)$ analytically.[36] The parameter V was evaluated numerically with the tip states being approximated by a hydrogenlike d function mimicking a tungsten tip.

Since the electronic structure of SWNTs near the Fermi energy is governed by the π states oriented perpendicularly to the nanotube walls, in our simulation, we employed a one-band tight-binding Hamiltonian which accounts for electron hopping beyond the first-neighbor approximation. Although other than π states may be present in the nanotube LDOS at the Fermi energy near defects,[12] the contributions from these states to the tunneling current are smaller than from the π states. This is because of smaller values of the corresponding tunneling matrix elements V (smaller spatial overlaps of the tip and any-other-than-π nanotube orbitals than the overlaps of the tip and π orbitals, as one can easily check by evaluating the overlap integrals, see Eq. (18) in Ref. 31). Moreover, there is strong evidence that this approximation works well for surface vacancies in graphite, as the comparison of simulated images[32,37] to the experimental ones[38] indicates. Thus, we believe that the STM images of nanotubes near defects may be qualitatively understood in terms of the simple picture of the π electrons. To allow for the dependence of the hopping elements on interatomic distances, we used the scaling functions given in Ref. 30

The recursion method[39,40] was employed to calculate the LDOS of a nanotube. STM images were computed for the

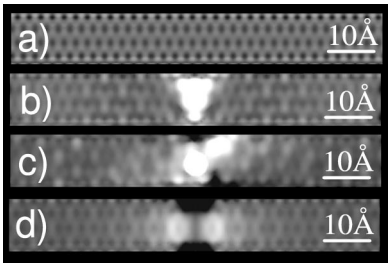

FIG. 4. STM gray-scale images of a pristine (10,10) nanotube (a) and the images of the same nanotube with the irradiation-induced defects as shown in Fig. 1. $V_{\text{bias}}=+0.2$ V. The defects are at the centers of the images.

constant current mode of STM operation, in which the height of the STM tip (the z coordinate) is adjusted to keep a constant value of current. To simulate this mode, we numerically solved Eq. (1) for the z coordinate at any scan point (x,y). The axis of the nanotubes coincided with the x axis. In order to achieve atomic corrugation, we subtracted the current profile above a SWNT averaged over the nanotube axis from the initial profile[23,33,34] (we ''filtered'' the image). As usual, brighter parts of the images stand for higher positions of the STM tip.

We present the STM images calculated for positive $V_{\text{bias}}=0.2$ V. Although there are quantitative differences between the STM images calculated at negative and positive values of V_{bias}, the overall forms of the patterns are roughly the same. Throughout this article, all lengths in the graphics are given in Å. All the STM images correspond to the topmost parts of the SWNTs (-5 Å $<y<5$ Å, the diameter of a (10,10) SWNT is ≈ 14 Å). Defects are always at the origin.

To establish a correspondence with the already published results, we start by plotting a gray-scale STM image of a perfect (10,10) armchair SWNT in Fig. 4(a). It is evident that the STM image of a pristine SWNT does not demonstrate a hexagonal network of carbon atoms in the graphene plane. Instead, a triangular lattice of darkish spots is seen. These spots correspond to the centers of hexagons. The image is in a perfect agreement with the experimental data[41–44] and the results of theoretical simulations.[6,8,45]

An STM image of the nanotube with a vacancy is presented in Fig. 4(b). The main feature of the STM image is a dramatic protrusion above the vacancy. Depending on the sign of V_{bias}, the height of the hillock is $\approx 0.7-0.8$ Å, while its linear size is independent of V_{bias} and constitutes ≈ 5 Å. As discussed earlier,[23,33,34] the enhancement in the tunneling current is due to vacancy-induced states near the Fermi energy (which may be interpreted as ''dangling bonds''), and these states are spatially localized on the atoms surrounding the vacancies. Since it is specifically these states which STM probes at small bias voltages, a vacancy is imaged as a protrusion. A similar effect has been reported for surface vacancies in graphite, see Refs. 32 and 46 and references therein.

Figure 4(c) shows an STM image of the SWNT with a 5-1db defect. Again, similar to the case of a vacancy, a hillocklike feature above the defect is evident. However, the shape of the feature is quite different from that in the case of the single vacancy. The hillock does not have a trigonal form typical for vacancy-induced protrusions since 5-1db defects have only one dangling bond, see Fig. 1(c). Besides this, an additional maximum is seen on the top-right of the main hillock. This feature stems from a perturbation in the electronic structure of the SWNT near the pentagon ring. Notice that an increase in the tunneling current above five-atom rings in STM images of nanotubes taken near SW defects has been also reported.[9] The height of the 5-1db-defect-induced hillock is roughly the same as that for the single vacancy and constitutes 0.8(0.4) Å for $V_{\text{bias}}=+0.2(-0.2)$ V.

The 5-6 defect, if it exists long enough to be measured by STM, also gives rise to a small bump in the STM image of the SWNT, see Fig. 4(d). The protrusion is also governed by electronic effects (a change in the electronic density distribution near E_F in the vicinity of pentagon rings) but not by the geometry of the defect, since the changes in atom coordinates in the direction perpendicular to the nanotube surface are minor. Moreover, the defect gives rise to a small dent on the nanotube surface. However, the decrease in the tunneling current due to the dent is compensated by the growth in the LDOS on the atoms in pentagons. As a result, the enhancement in the tip height is smaller as compared to those for the other defects, less than 0.3 Å. The shape of the hillock reflects the symmetry of the underlying atomic structure of the defect, cf. Fig. 1(d). The overall shape of the hillock is similar to that for a SW defect,[6–8] formed by two pentagons and two heptagons (in our nomenclature, a ''5-7'' defect) although we stress that we have quite a different atomic structure here, since one carbon atom is missing. However, we did not observe formations of SW defects under ion irradiations. Thus, such features in the STM images of irradiated nanotubes, as in Fig. 1(d), should be related to 5-6 defects rather than SW defects.

Note that, together with the network of dark spots, modulations in h along the nanotube axis are present near the vacancy and 5-1db defects. These modulations, or superstructures, with a period commensurate with (but larger than) that of the underlying graphene lattice also stem from electronic effects.[23] Thus, our simulations confirm predictions[47] on the anisotropy of STM images near point defects on nanotube walls and specify the shape of the superstructures resulting from irradiation-induced small-scale defects.

Since the spectroscopic mode of STM operation can also provide unique data on the local electronic structure of nanotubes and facilitate distinguishing the defects, we further simulated current-to-voltage ($I-V$) characteristics of nanotubes near all the defects. Within the framework of our model, the $I-V$ curves are actually the LDOSs on carbon atoms nearest the STM tip averaged with the weights determined by the corresponding tip-surface matrix elements. For all the defects, $I-V$ curves were calculated at the points in the $x-y$ plane corresponding to maximum tunneling currents.

For the sake of comparison, in Fig. 5(a) we plot the $I-V$ curve calculated at a distance from a defect, and this coincides with the $I-V$ curve for a pristine (10,10) nanotube. We

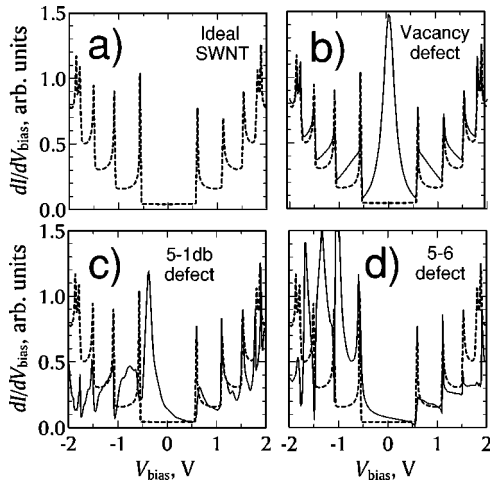

FIG. 5. $I-V$ curves for a (10,10) pristine nanotube (a) and calculated above the same nanotube with the irradiation-induced defects (b)–(d) as shown in Fig. 1. The $I-V$ curves for the pristine nanotube (dashed lines) are also plotted in (b)–(d).

did not allow for a possible shift of E_F (Ref. 48) (of about 0.2 eV) due to the charge transfer from the substrate, which leads to an asymmetric position of the nanotube band structure of perfect SWNT's relative to E_F. Although charge transfer has been reported in Ref. 48, other experimental studies[41,49] indicate that the SWNT-substrate interaction is rather small. In any case, our theoretical STM images are slightly dependent on the possible shift of the E_F position. As for the scanning-tunneling spectrum (STS) curves, this effect just shifts the entire curves along the bias voltage axis.

Figure 5(b) presents an $I-V$ curve calculated above a vacancy. As evident from the figures, the vacancy results in a sharp increase in the LDOS at the E_F on atoms nearest the vacancy (this increase, in its turn, gives rise to a hillocklike feature in the corresponding STM image). If there is no charge transfer from the substrate, then the plot is practically symmetrical relative to the position of E_F.

A sharp maximum is also evident in the $I-V$ curve for the 5-1db defect, see Fig. 5(c). This peak originates from the dangling bond. However, since the local symmetry of the graphene plane is broken near this defect, the position of the peak does not coincide with that of E_F. This explains the asymmetry in the hillock height for positive and negative bias voltages.

As follows from the $I-V$ curve for the 5-6 defect, Fig. 5(d), the increase in LDOS near the defect is not as strong as compared to those for the other defects, which explains why the hillock is rather flat in this case. We stress here once more that we consider the limit of small bias voltages: as follows from Fig. 5(d), STM images might be quite different at larger bias voltages $V_{\text{bias}}>1$ V, when the states distanced from E_F contribute to the tunneling current. However, since our technique works well only for the limit of small V_{bias},[31] we did not simulate STM images of defects at large V_{bias}.

It is noteworthy that the features in the STM images of nanotubes with defects—hillock-like features and electronic superstructures—have been observed earlier in experimental STM images of graphite surfaces with vacancies.[38,50]

IV. CONCLUSIONS AND SUGGESTIONS FOR POSSIBLE EXPERIMENTS

In this article, we simulated time evolution of atomic-scale defects produced by low-dose irradiation of nanotubes with Ar ions. Since vacancies are the most prolific defects which appear under low-dose, low temperature irradiation,[23] we computed the lifetimes of the vacancies and vacancy-related defects (those are 5–6 and 5-1db defects, the latter having the minimum energy among all three defect configurations). Our calculations indicate that at low temperatures single vacancies and the 5–6 defects are likely stable on macroscopically long time scales and, hence, they might be experimentally found.

Inasmuch as STM is a powerful tool for both the characterization of atom-scale defect and the study of their time evolution, we also calculated STM images and current-to-voltage characteristics of irradiated nanotubes, employing for this the tight-binding Green's function technique. We demonstrated that these defects may be detected by STM and that, at low bias voltages, all of them appear as hillocklike features in constant-current mode STM images due to the growth in the local electron density of states on atoms surrounding the defects.

The shape and dimensions of the hillocks as well as the current-to-voltage characteristics vary for different defects, which makes it potentially possible to experimentally distinguish such defects using STM. To minimize the effect of the STM tip on the electronic subsystem and to avoid mechanical deformation, such experiments should be carried out at maximum possible tip-surface separations and at low bias voltages.

Since vacancies in nanotubes, unlike vacancies in graphite, seem to be metastable, atomic-resolution STM probing of irradiated nanotubes at different temperatures immediately after irradiation may be of particular interest. The main goals of these possible STM experiments would be (i) to find by STM indications of irradiation-induced changes in nanotubes, (ii) to identify the types of irradiation-induced defects for low irradiation doses and low energies of incident ions by comparing experimental STM images and spectra to theoretical ones, and (iii) to study the stability and evolution of defects by varying temperature and by observing changes in STM images.

The experiments on irradiating nanotubes with inert gas ions and subsequent STM probing, if carried out, may enable one to observe the temporal evolution of irradiation-induced defects at various temperatures and compare experimental lifetimes to those predicted theoretically. Thus, such experiments, although being a challenging task, may not only contribute to understanding the mechanisms of defect formation, but may also serve as a test for the validity of tight-binding and empirical potential molecular dynamics models.

In summary, we studied the behavior of atomic-scale defects produced by low-dose irradiation of nanotubes with Ar

ions and computed their lifetimes at various temperatures. We demonstrated that at low temperatures the defects are likely stable on macroscopically long timescales and appear as hillock-like features in STM images due to the growth in the local electron density of states on atoms surrounding the defects. Since the shape of the hillocks are different for different defects, they might be experimentally distinguished using STM.

ACKNOWLEDGMENTS

The authors would like to thank E. Salonen for valuable discussions. The research was supported by the Academy of Finland under Project Nos. 44215 and 73722. Grants of computer time from the Center for Scientific Computing in Espoo, Finland are gratefully acknowledged.

[1]C. Dekker, Phys. Today **52**, 22 (1999).
[2]P. L. McEuen, Nature (London) **393**, 15 (1998).
[3]S. J. Tans, A. R. M. Verscheueren, and C. Dekker, Nature (London) **393**, 49 (1998).
[4]Z. Yao, H. Postma, L. Balents, and C. Dekker, Nature (London) **402**, 273 (1999).
[5]M. Bockrath, W. Liang, D. Bozovic, J. H. Hafner, C. M. Lieber, M. Tinkham, and H. Park, Science **291**, 283 (2001).
[6]J.-C. Charlier, T. W. Ebbesen, and P. Lambin, Phys. Rev. B **53**, 11 108 (1996).
[7]V. Meunier and P. Lambin, Carbon **38**, 1729 (2000).
[8]A. Rubio, Appl. Phys. A: Mater. Sci. Process. **68**, 275 (1999).
[9]D. Orlikowski, M. B. Nardelli, J. Bernholc, and C. Roland, Phys. Rev. B **61**, 14 194 (2000).
[10]D. Orlikowski, H. Mehrez, J. Taylor, H. Guo, J. Wang, and C. Roland, Phys. Rev. B **63**, 155 412 (2001).
[11]Y. Xia, Y. Ma, Y. Xing, Y. Mu, C. Tan, and L. Me, Phys. Rev. B **61**, 11 088 (2000).
[12]H. J. Choi, J. Ihm, S. Louie, and M. Cohen, Phys. Rev. Lett. **84**, 2917 (2000).
[13]L. Chico, L. X. Benedict, S. G. Louie, and M. Cohen, Phys. Rev. B **54**, 2600 (1996).
[14]A. Hansson, M. Paulsson, and S. Stafström, Phys. Rev. B **62**, 7639 (2000).
[15]T. Kostyrko, M. Bartkowiak, and G. D. Mahan, Phys. Rev. B **60**, 10 735 (1999).
[16]M. Igami, T. Nakanishi, and T. Ando, Physica B **284-288**, 1746 (2000).
[17]D. Orlikowski, M. B. Nardelli, J. Bernholc, and C. Roland, Phys. Rev. Lett. **83**, 4132 (1999).
[18]C.-H. Kiang, W. Goddard, R. Beyers, and D. Bethune, J. Phys. Chem. **100**, 3749 (1996).
[19]P. M. Ajayan, V. Ravikumar, and J.-C. Charlier, Phys. Rev. Lett. **81**, 1437 (1998).
[20]M. Terrones, H. Terrones, F. Banhart, J.-C. Charlier, and P. M. Ajayan, Science **288**, 1226 (2000).
[21]F. Banhart, Rep. Prog. Phys. **62**, 1181 (1999).
[22]H. Stahl, J. Appenzeller, R. Martel, P. Avouris, and B. Lengeler, Phys. Rev. Lett. **85**, 5186 (2000).
[23]A. V. Krasheninnikov, K. Nordlund, M. Sirviö, E. Salonen, and J. Keinonen, Phys. Rev. B **63**, 245 405 (2001).
[24]Y. Zhu, T. Yi, B. Zheng, and L. Cao, Appl. Surf. Sci. **137**, 83 (1999).
[25]M. P. Allen and D. J. Tildesley, *Computer Simulation of Liquids* (Oxford University Press, Oxford, 1989).
[26]D. W. Brenner, Phys. Rev. B **42**, 9458 (1990).
[27]J. N. Glosli and H. Ree, J. Chem. Phys. **110**, 441 (1999).
[28]C. Journet, W. K. Maser, P. Bernier, A. Loiseau, M. L. de la Chapelle, S. Lefrant, P. Deniard, R. Lee, and J. E. Fischer, Nature (London) **388**, 756 (1997).
[29]M. B. Nardelli, B. I. Yakobson, and J. Bernholc, Phys. Rev. B **57**, 4277 (1998).
[30]C. Xu, C. Wang, C. Chan, and K. Ho, J. Phys.: Condens. Matter **4**, 6047 (1992).
[31]B. McKinnon and T. Choy, Phys. Rev. B **54**, 11 777 (1996).
[32]A. V. Krasheninnikov and V. F. Elesin, Surf. Sci. **454-456**, 519 (2000).
[33]A. V. Krasheninnikov, Phys. Low-Dimens. Semicond. Struct. **11/12**, 1 (2000).
[34]A. V. Krasheninnikov, Solid State Commun. **118**, 361 (2001).
[35]J. Bardeen, Phys. Rev. Lett. **6**, 57 (1961).
[36]E. Economou, *Green's Functions in Quantum Physics* (Springer, Berlin, 1979).
[37]K. F. Kelly and N. J. Halas, Surf. Sci. **416**, L1085 (1998).
[38]J. G. Kushmerick, K. F. Kelly, H.-P. Rust, N. J. Halas, and P. S. Weiss, J. Phys. Chem. **103**, 1619 (1999).
[39]R. Haydock, Solid State Phys. **35**, 216 (1980).
[40]C. M. Goringer, D. R. Bowler, and E. Hernández, Rep. Prog. Phys. **60**, 1447 (1997).
[41]M. Ouyang, J. L. Huang, C. L. Cheung, and C. M. Lieber, Science **292**, 702 (2001).
[42]J. W. G. Wildöer, L. Venema, A. G. Rinzler, R. E. Smalley, and C. Dekker, Nature (London) **391**, 59 (1998).
[43]T. W. Odom, J. L. Huang, P. Kim, and C. M. Lieber, Nature (London) **391**, 62 (1998).
[44]A. Hassanine, M. Tokumoto, Y. Kumazawa, H. Kataura, Y. Maniwa, S. Suzuki, and Y. Achiba, Appl. Phys. Lett. **73**, 3839 (1998).
[45]V. Meunier and P. Lambin, Phys. Rev. Lett. **81**, 5588 (1998).
[46]K. Nordlund, J. Keinonen, and T. Mattila, Phys. Rev. Lett. **77**, 699 (1996).
[47]C. L. Kane and E. J. Mele, Phys. Rev. B **59**, 12 759 (1999).
[48]L. C. Venema, J. W. Janssen, M. R. Buitelaar, J. W. G. Wildöer, S. G. Lemay, L. P. Kouwenhoven, and C. Dekker, Phys. Rev. B **62**, 5238 (2000).
[49]M. S. Dresselhaus, Science **292**, 650 (2001).
[50]J. Hahn and H. Kang, Phys. Rev. B **60**, 6007 (1999).